Nano Research

ISSN 1998-0124 CN 11-5974/O4
https://doi.org/10.26599/NR.2026.94908467

Research Article

Understanding and regulation of stress-induced structural evolution in silicon anodes for high-energy-density batteries

Xiangrui Duan§, Yangtao Ou§, Shuibin Tu, Wenyu Wang, Hengtao Shen, Guocheng Li, Yuanjian Li, Junjie Fu, Ruikang Feng, Renming Zhan, Yongming Sun(✉)
Wuhan National Laboratory for Optoelectronics, Huazhong University of Science and Technology, Wuhan 430074, China
§ Xiangrui Duan and Yangtao Ou contributed equally to this work.

Nano Res., **Just Accepted Manuscript** • https://doi.org/10.26599/NR.2026.94908467
https://www.sciopen.com/journal/1998-0124 on Jan. 21, 2026

Just Accepted

TABLE OF CONTENTS (TOC)

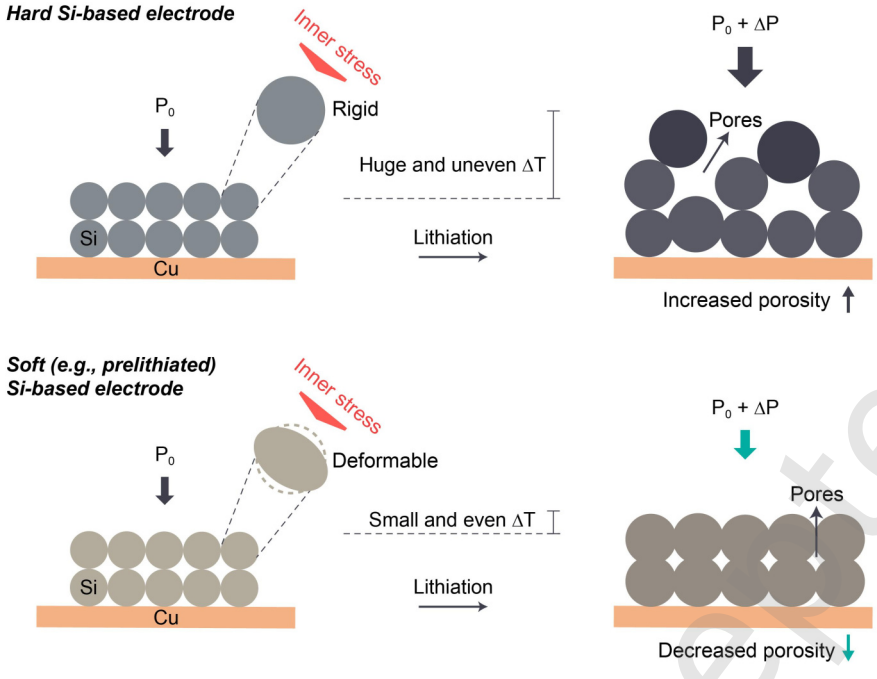

Beyond supplying Li, prelithiation critically regulates the electrochemo-mechanical behavior of Si-based anodes by harnessing lithiation-induced internal stress to densify the electrode structure, thereby improving both cycling stability and energy density in lithium-ion batteries.

Nano Research

Open Access

Research Article

Understanding and regulation of stress‐induced structural evolution in silicon anodes for high-energy-density batteries

Xiangrui Duan§, Yangtao Ou§, Shuibin Tu, Wenyu Wang, Hengtao Shen, Guocheng Li, Yuanjian Li, Junjie Fu, Ruikang Feng, Renming Zhan, and Yongming Sun ✉

Wuhan National Laboratory for Optoelectronics, Huazhong University of Science and Technology, Wuhan, 430074, China
§ Xiangrui Duan and Yangtao Ou contributed equally to this work.

Received: 24 September 2025; **Revised:** 13 November 2025; **Accepted:** 21 January 2026

✉ Address correspondence to yongmingsun@hust.edu.cn

Cite this article: *Nano Research*, **2026**, *19*, 94908467. https://doi.org/10.26599/NR.2026.94908467

ABSTRACT: Silicon (Si)-based electrodes are widely regarded as a promising anode option for next-generation high-energy batteries. Although the substantial volume expansion during charge/discharge cycles is recognized as a primary cause of Si-based anode failure, the correlation between material volume changes, electrode-scale electrochemical-mechanical behavior, and electrochemical performance remains unclear. This poses a significant obstacle to the design of high-performance Si-based anodes. Herein, by combining operando detection of spatial stress in pouch cells (8 × 8 cm) with materials characterization, we elucidate the dependence of electrochemical performance on the inner stress-driven structural evolution of Si-based anodes, where large, uneven stress/strain dominates their mechanical degradation, compromising electrochemical reversibility. Significantly, we unveil that, beyond the basic function of Li compensation, prelithiation redirects the stress-induced structural evolution of the electrode from pore and crack formation to a void-filling-dominated process, effectively mitigating volume changes and reaction inhomogeneity. With ~25% prelithiation degree of the anode, $LiCoO_2$||Si/C pouch cells, featuring an anode specific capacity of ~1300 mAh g^{-1} and areal capacity of ~2.3 mAh cm^{-2}, deliver a remarkable reduction in anode porosity of 14.4% during the initial charge, in contrast to a 5.4% increase in the unprelithiated counterpart. Synchronously, electrode swelling diminishes from over 153% to below 18%. Harnessing this favorable electrochemical-mechanical behavior, the pouch cell delivers a 27.1% improvement in capacity retention after 200 cycles at 0.5 *C*, outside of a 90.4% increase in cumulative discharge capacity.

KEYWORDS: Si-anode pouch cells, high energy density, electrochemical-mechanical behavior, structural evolution, operando spatial stress measurement

1 Introduction

Silicon (Si) anodes have emerged as a leading candidate for high-energy-density lithium-ion batteries (LIBs) due to their high specific capacity (3579 mAh g^{-1} for $Li_{15}Si_4$) and suitable operating voltage (~0.4 V vs. Li^+/Li) [1-4]. However, they face significant challenges, primarily due to the large volume swing (up to 100% at the electrode level) upon (de)lithiation processes [5-7], a consequence of the high Li^+ storage per unit mass of the active material. This unfavorable mechanical behavior leads to material fracture, electrode pulverization, delamination from the current collector, and severe stress-strain fluctuations at both the electrode and cell levels, ultimately causing the rapid failure of LIBs with Si-based anodes [8, 9].

To date, various strategies such as material design [10-12], electrode architecture [13-16], and electrolyte formulation [17, 18] have been developed to mitigate the volumetric fluctuations of Si-based anodes and their adverse effects on electrochemical performance. Despite notable progress in improving material stability [19-21], the electrochemical-mechanical behavior of Si-based anodes during cycling in practical pouch cells, along with the underlying mechanisms, remains poorly understood—let alone their influence on battery performance under real-world conditions. This underscores the critical importance of investigating and integrating electrode/battery engineering [22, 23]. Specifically, when materials undergo repeated large volume fluctuations, it is essential to thoroughly investigate the expansion and mechanical stability at the electrode scale, the evolution of electrode structure, and the stress-strain responses at the battery scale. These aspects are crucial for maintaining continuous electronic and ionic transport pathways during cycling and safeguarding stable battery operation [24, 25].

Conducting systematic operando studies on the spatial and temporal stress-strain behavior, as well as the structural evolution of large-scale Si-based electrodes, is of great significance in understanding their electrochemical-mechanical behavior and promoting their performance improvement. Such an approach could help revisit and unravel the intricate mechanisms underlying various strategies from an electro-chemo-mechanics perspective, and pave the way for the development of refined approaches to enhance battery performance. Thus far, local stress/strain characteristics in Si-

based batteries have been probed using fiber-type sensors [26, 27] at the material scale or point-style sensors [28, 29] at the electrode scale. Yet, a detailed investigation into the full-spectrum electrochemical-mechanical behavior across the entire Si-based anode, along with its implications for practical pouch cells, remains largely unexplored.

In this study, we systematically investigated the real-time strain-stress behavior during the operation of Si-based laminated pouch cells (8 × 8 cm) by an operando spatial stress mapping technique, and quantitatively analyzed the electrode structure evolution in terms of thickness, porosity, and homogeneity. We then established the correlation between inner stress-driven structural evolution and electrochemical behavior of Si-based anodes in pouch cells. Furthermore, we unraveled the advanced role of prelithiation in manipulating the electrochemical-mechanical behavior of Si-based anodes, apart from its Li-replenishment feature, which exploited the inner stress to densify electrode structure during lithiation. For demonstration, the anode thickness in a $LiCoO_2$||Si/C pouch cell with an anode specific capacity of ~1300 mAh g^{-1} and areal capacity of ~2.3 mAh cm^{-2} expanded by over 153% after the initial charge, accompanied by a 5.4% increase in porosity and the formation of numerous cracks, indicating pronounced heterogeneity. In contrast, Si/C anode with ~25% degree of prelithiation delivered a desirable 14.4% reduction in porosity post-charging under identical conditions, effectively limiting thickness expansion to below 18%. Meanwhile, prelithiation reduced the average pressure deviation per unit of charge (dP/dQ) during the alloying process by ~72%, decreasing from 0.64 to 0.18 kPa mAh^{-1}, and significantly improved reaction homogeneity. Consequently, notable improvements of 27.1% in capacity retention and 90.4% in cumulative discharge capacity were synchronously achieved after 200 cycles at 0.5 *C* in the practical pouch cells.

2 Results and discussion

2.1 Stress and strain analysis model of Si-based full pouch cells

In Si-anode full pouch cells (see Scheme 1a), the thickness expansion of Si-based anodes during lithiation (> 100%) far surpasses that of conventional cathodes, such as lithium nickel manganese cobalt oxide (NMC) (~1%) and lithium cobalt oxide (LCO) (~0.3%) (see Scheme 1b) [28, 30, 31]. Consequently, the anode inherently governs the overall thickness fluctuations of the battery. To illustrate this, we conducted a thickness analysis on a laminated pouch cell comprising an NMC cathode and a Si-based anode, with an

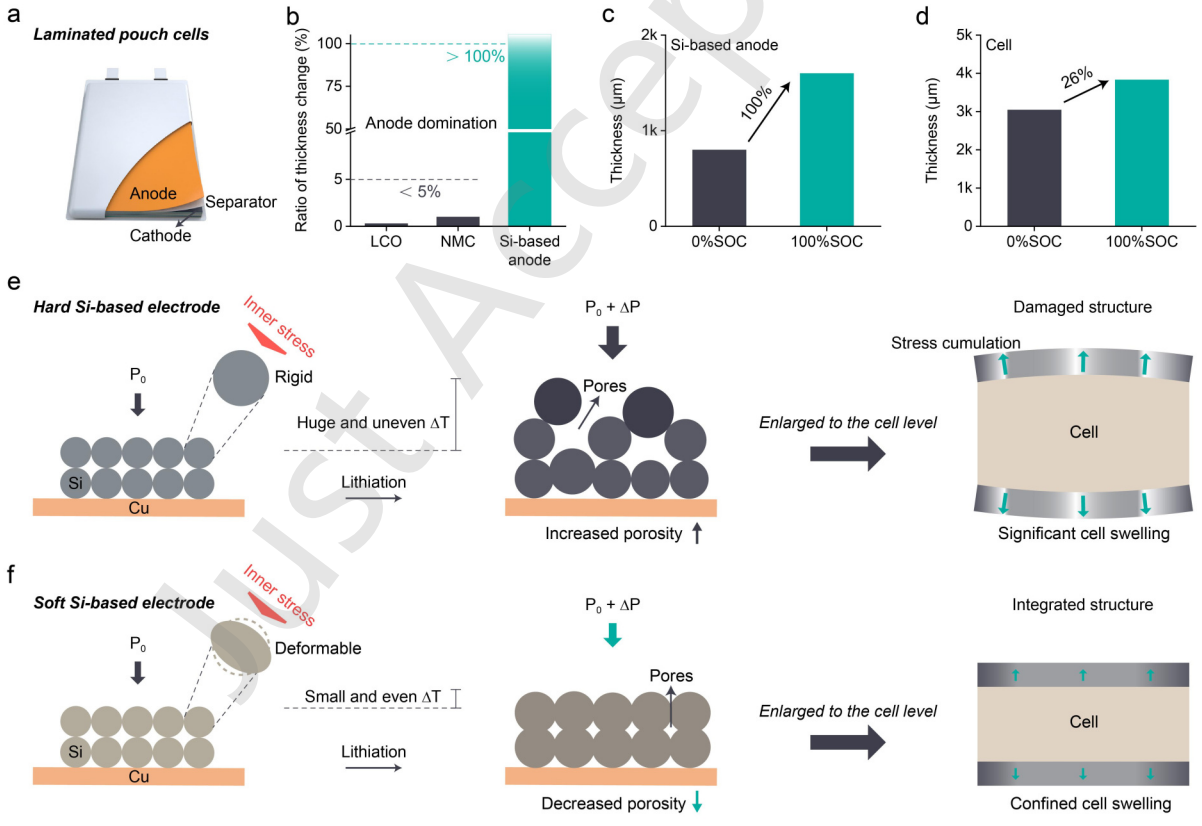

Scheme 1. Stress and strain analysis of Si-based laminated pouch cells. (a) Schematic of a Si-based laminated pouch cell. **(b)** Thickness change ratios of typical cathodes and Si-based anode between the fully charged and discharged states of batteries. **(c, d)** Thickness of a Si-based anode **(c)** and the corresponding cell **(d)**, at 0% and 100% state of charge (SOC) in a pouch cell with anode capacity of 4 mAh cm^{-2} and lamination number of 10. **(e, f)** Schematic of the inner stress-driven structural evolution during lithiation for Si-based anodes **(e)** without and **(f)** with prelithiation. Prelithiated Si-based anode material possesses lower rigidity and better deformability in comparison to the bare material. Upon lithiation, the "hard" (non-deformable) Si-based anode undergoes enormous and non-uniform volume expansion, resulting in increased porosity at the electrode level, and structural deformation at the cell level. In contrast, the "soft" (deformable) Si-based anode exhibits restricted and uniform volume dilation, yielding a densified electrode structure and integrated cell structure

areal capacity of ~4 mAh cm^{-2} and a lamination number of 10 (see Scheme 1c, d, and Table S1). Upon charging to 100% state of charge (SOC), the cell thickness increased from 3046 to 3832 μm, accompanied by a doubling of the anode thickness from 800

to 1600 μm. This corresponds to a ~26% increase at the cell level, which aligns with a 100% expansion at the Si-based anode level upon full lithiation. As such, the volumetric changes of Si-based anodes dictate the overall dimensional evolution of the cell and can be systematically probed via operando spatial pressure mapping at the cell scale.

As depicted in Scheme 1e, the Si-based anode is typically characterized by its rigid nature [32, 33], which imparts resistance to deformation during the initial operation. Upon charge (lithiation), it undergoes catastrophic volume expansion, resulting in substantial and uneven changes in thickness (ΔT) and internal pressure (ΔP), along with increased electrode porosity. This behavior compromises the mechanical integrity of the anode and exacerbates parasitic reactions, contributing to capacity loss through the formation of isolated active materials and solid electrolyte interphase (SEI). At the cell level, excessive swelling imposes considerable stress on the mechanical constraints. As cycling progresses, this internal stress accumulates, intensifies, and ultimately jeopardizes the structural stability of the battery system, thereby increasing the risk of battery failure and raising significant safety concerns within individual batteries or battery modules. In contrast, the implementation of a Si-based electrode design with a "soft" (deformable) character (e.g., prelithiated Si-based anode with reduced Young's modulus and hardness, from ~92 GPa and ~5 GPa to ~12 GPa and ~1.5 GPa, respectively [34, 35]) can enable inner stress-driven structural adaptation, thereby significantly restricting and homogenizing the anode's volume response to Li-ion intake. This design leads to lower and more uniform ΔT and ΔP during lithiation, accompanied by a densified electrode structure with reduced porosity, effectively mitigating cell swelling. Consequently, the internal pressure buildup of the battery system is suppressed and structural integrity is preserved, ensuring long-term stable and safe battery operation.

2.2 *Operando spatial stress evolution of Si-based full pouch cells*

To monitor the mechanical response during the charge/discharge processes of Si-based pouch cells, a real-time spatial stress mapping setup was established using a force-sensor film (Figure 1a and Figure S1). This film, with a smooth surface and dimensions of 8 × 8 cm (matching the cell size), consists of an ordered array of 1600 sensor nodes arranged in a 40 × 40 matrix. It is affixed to a mechanical constraint, along with the laminated pouch cell and a spring component. During cell operation, thickness variations (ΔT) induce elastic deformation in the spring component in the opposite direction, generating a corresponding pressure response (ΔP) governed by Hooke's law ($\Delta P = k\Delta T$, where k is a constant for a given compressed zone). This pressure fluctuation is captured in operando by the tightly fitted force-sensor film (Figure 1b). Given that ΔT is primarily dictated by the anode side, this system connects the spatiotemporal variations in thickness with stress evolution, enabling precise tracking of volume changes across the entire Si-based anode.

To investigate the electrochemical-mechanical behavior of Si-based anodes and the influence of the commonly adopted prelithiation process, we utilized a 250 mAh-level LCO (~2.1 mAh cm^{-2}) ||Si/C (~2.3 mAh cm^{-2}) laminated pouch cell configuration, featuring an anode with a mass loading of ~1.8 mg cm^{-2} and a specific capacity of ~1300 mAh g^{-1}. The cells' initial coulombic efficiency (ICE) and stress/strain response were evaluated during the first cycle at 0.1 *C*. Following a straightforward contact prelithiation process [36, 37], the cell incorporating a prelithiated Si/C anode (pre-Si/C) with a ~25% degree of prelithiation achieved a significantly improved ICE of 94.5%, surpassing the 65.8% observed in the unprelithiated counterpart (Figure 1c). This outcome validates the effectiveness of anode prelithiation in Li compensation. Synchronously, the pressure profiles of these cells as a function of state of charge (SOC) were monitored and presented in Figure 1d. Within the LCO||Si/C pouch cell, the internal pressure sharply climbed to 706.8 kPa upon full charge (completion of lithiation), starting from an initial value (P_0) of 542.3 kPa. This resulted in a significant pressure variation (ΔP) of 164.5 kPa and a growth rate of 30.3% relative to P_0. During discharging, the ΔP decreased with a deceleration trend, presumably due to the uneven dealloying process, and eventually reached a final value of 100.2 kPa (18.5% relative to P_0) (Figure S2). This pressure trajectory reflects a substantial volume change of the Si/C anode over the initial cycle. In contrast, the cell with pre-Si/C electrodes (P_0 = 531.5 kPa) exhibited a slow and steady stress evolution during the initial cycle under identical conditions. The ΔP reached 49.1 kPa (9.2% relative to P_0) at the end of charge, and further decreased to 39.4 kPa (7.4% relative to P_0) at the end of discharge. The limited pressure increase indicates restrained volume expansion of the pre-Si/C anode during cycling, attributable to the improved deformability of prelithiated active material. These findings underscore the critical role of prelithiation in regulating the electrochemical-mechanical behavior of Si-based electrodes, highlighting its substantial effect on structural stability and electrochemical reversibility.

The pressure deviation per unit of charge (dP/dQ) was introduced as a measure to quantify the rate of stress growth [31, 38]. As shown in Figure 1e, the LCO||Si/C pouch cell exhibited a highly fluctuating trajectory of dP/dQ with an average of 0.64 kPa mAh^{-1} during charging and -0.38 kPa mAh^{-1} during discharging. This erratic evolution of stress reflects the unstable mechanical behavior of the Si/C electrode, resulting in huge and uneven volume fluctuations. In contrast, the incorporation of a pre-Si/C anode transformed the stress evolution into a steady pattern, maintaining a low and stable dP/dQ plateau of 0.18 kPa mAh^{-1} during charging and -0.05 kPa mAh^{-1} during discharging. This well-regulated stress response is attributed to the restricted volume change during Li^+ insertion/extraction in the pre-Si/C particles, contributing to a stabilized electrode structure. Post-mortem examinations of the anode at fully charged and discharged states were conducted to further elucidate the impact of prelithiation on strain evolution (Figure 1f). Following the initial lithiation, the average thickness of the Si/C electrode experienced a significant increase from ~30 to ~76 μm (Figure S3 and S4), displaying high non-uniformity and a swelling ratio of 153%. Upon delithiation, the electrode contracted to an average thickness of ~60 μm, corresponding to a swelling rate of 100%, and exhibited a porous, fractured structure (Figure S5). These observations align with the abovementioned stress analysis results, highlighting the mechanical instability of Si-based anodes. Interestingly, the large-size pre-Si/C anode (8 × 8 cm) demonstrated well-constrained volume variation throughout alloying/dealloying, with average thicknesses of approximately

39, 46, and 41 μm at 0%SOC, 100%SOC, and 100% depth of discharge (DOD), respectively. This corresponds to low swelling ratios of 18% post-charging and 5% post-discharging, thereby preserving a dense and intact electrode structure. These observations confirm that prelithiation modulates stress-strain evolution in Si-based anodes, extending beyond Li compensation to concurrently enhance electrochemical reversibility and energy density.

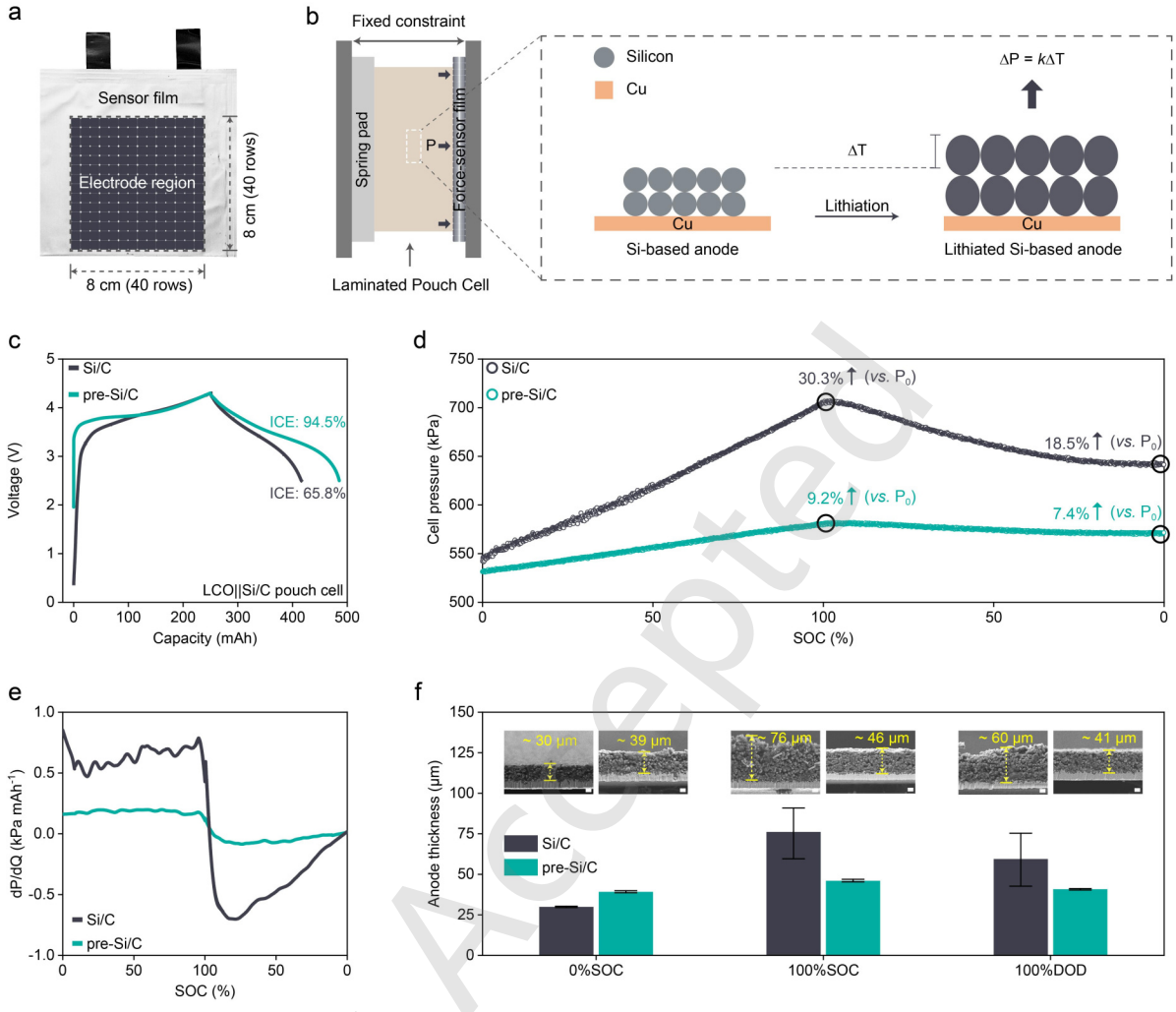

Figure 1. Spatiotemporal stress response to strain of the Si-based anode in LCO||Si/C laminated pouch cells during operation. (a) Photograph of the LCO||Si/C laminated pouch cell with an 8 × 8 cm stress test region. The inset displays a schematic of the force-sensor film, featuring an ordered array of 40 × 40 rows (1600 sensor nodes). **(b)** Scheme of the spatiotemporal stress measurement setup, where a sensor film, laminated pouch cell, and spring component are clamped onto a mechanically fixed constraint. The zoomed-in view provides a detailed understanding of the relationship between pressure variation and thickness change in a specific electrode area. **(c)** Voltage profiles of the cell with and without anode prelithiation during the initial cycle at 0.1 *C* and **(d)** the corresponding operando stress evolution. **(e)** The dP/dQ profiles of the cell during the initial charge/discharge cycle, before and after anode prelithiation. **(f)** Anode thickness of the cell, with and without anode prelithiation, at 0%SOC, 100%SOC, and 100% depth of discharge (DOD). The error bars represent the range between a pair of values measured at disparate locations (n = 3) within each laminated pouch cell, with the data point signifying the mean value. Inset shows the corresponding typical cross-sectional SEM images for each state. Scale bars, 10 μm

2.3 *Homogeneity of stress/strain evolution in Si-based full pouch cells*

To visualize the volume change across the entire electrode, the three-dimensional spatial distribution of ΔP was reconstructed from the pressure matrix. A blue-to-red color gradient was employed, with red denoting regions of elevated ΔP corresponding to pronounced volume dilation. As depicted in Figure 2a, the ΔP topography for the LCO||Si/C pouch cell at 100%SOC exhibited intense oscillation, characterized by a high standard deviation (SD) value of 167.2. Different locations within the large-size Si/C anode exhibited varying ΔP values, demonstrating spatial heterogeneity. In contrast, the LCO||pre-Si/C pouch cell displayed a much smoother ΔP morphology after charging, with minimal undulations and a significantly lower SD value of 30.6 (Figure 2b), indicating a more uniform and confined volume expansion.

To further investigate the interregional discrepancy in stress evolution, three representative zones (R1, R2, and R3, each with dimensions of 1 × 1 cm) were selected along the electrode diagonal (Figure 2c,d). Upon charging the LCO||Si/C pouch cell, diverse pressure growth patterns emerged: R1 exhibited a moderate final ΔP of 201.9 kPa following an accelerated increase, R2 showed a steeper rise culminating at 310.9 kPa, while R3 displayed a more gradual increase, reaching only 116.2 kPa. Meanwhile, the thickness of the anode expanded to ~78, ~91, and ~60 μm, respectively, from an initial baseline of ~30 μ m (Figure S4a). These disparities reflect non-uniform

electrochemical reactions, yielding markedly different anode swelling ratios of 160%, 203%, and 99% for R1, R2, and R3, respectively (Figure 2e). By contrast, the LCO||pre-Si/C pouch cell exhibited nearly identical pressure growth trajectories across all three regions, with final ΔP values of 56.4, 58.4, and 52.2 kPa at 100%SOC, respectively. Notably, the thicknesses of the pre-Si/C anode in regions R1, R2, and R3 expanded slightly to approximately 46, 47, and 45 μm after lithiation, respectively, from an initial baseline of ~39 μm, corresponding to constrained swelling ratios of 17%, 20%, and 16% (Figure 2f and Figure S4b). These findings substantiate the effectiveness of anode prelithiation in facilitating a well-densified and homogenized alloying process across the large-scale Si-based electrode.

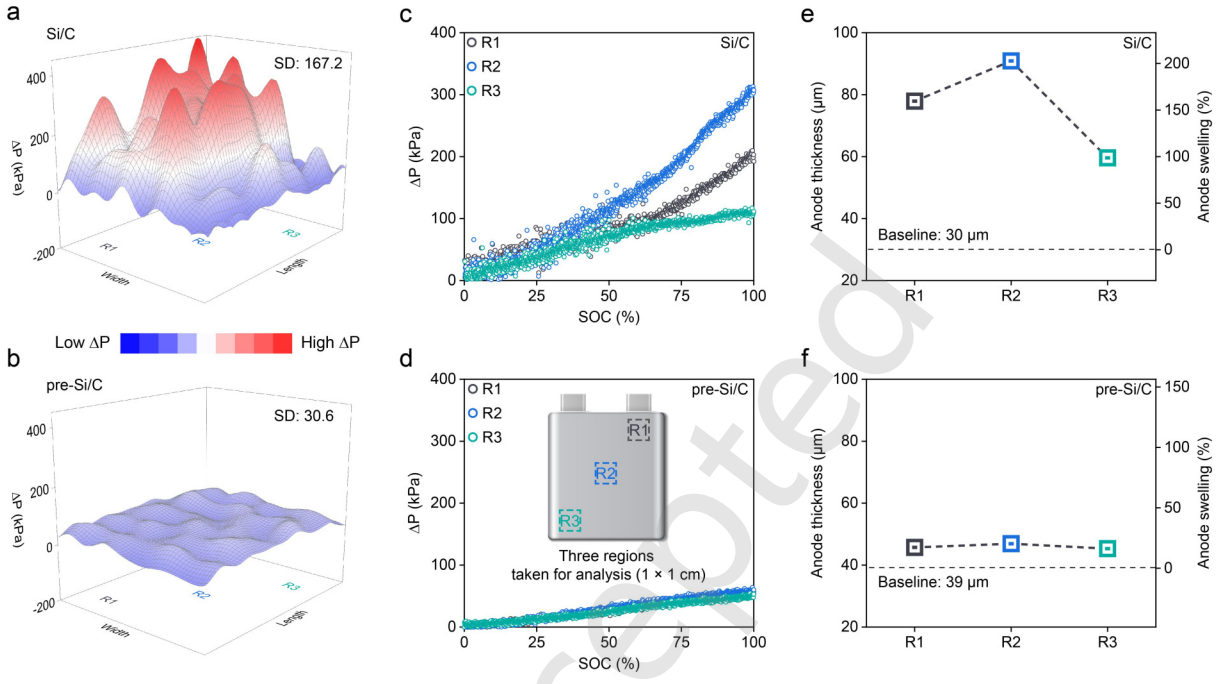

Figure 2. Homogeneity of stress and strain evolution in LCO||Si/C laminated pouch cells without and with anode prelithiation. (a, b) Three-dimensional spatial distribution of ΔP following the initial charge at 0.1 *C* for **(a)** LCO||Si/C and **(b)** LCO||pre-Si/C pouch cells. Red represented higher ΔP than blue in the heat map. **(c, d)** Pressure evolution in three zones (R1, R2, and R3), each measuring 1 × 1 cm and arranged along the diagonal of the cell, during the initial charge at 0.1 *C*, **(c)** without and **(d)** with anode prelithiation. Inset illustrates the selected three zones across the cell. **(e, f)** Electrode thickness and the corresponding swelling ratio in three regions, R1, R2, and R3, of the anode after the 1st lithiation at 0.1 *C*, without **(e)** and with **(f)** anode prelithiation.

2.4 *Structural evolution mechanism of Si-based anodes during battery charging*

To elucidate the mechanism by which prelithiation modulates stress – strain behavior in Si-based electrodes, post-mortem three-dimensional X-ray computed tomography (CT) with micron-level resolution was employed. This technique enabled direct quantification of electrode structure evolution during charging, including thickness and porosity [39, 40]. As shown in Figure 3a, the pristine Si/C anode with a capacity of ~2.3 mAh cm^{-2} exhibited an initial thickness of 30.0 μm and a porosity of 22.4% within a region measuring 160.0 × 200.0 μm. Upon full lithiation, the anode thickness sharply expanded to 59.8 μm, accompanied by a 5.4% increase in porosity, reaching 27.8%. In contrast, the pre-Si/C anode exhibited significantly restrained thickness expansion during charging, measuring 39.2 μm at 0%SOC and 45.7 μm at 100%SOC (Figure 3b). Simultaneously, its porosity decreased markedly by 14.4%, from 24.6% to 10.2% (Figure 3c), indicating a more compact and densified electrode structure. From a mechanical standpoint, the substantial swelling and increased porosity of the lithiated Si/C electrode suggest that a predominant vertical growth mode occurs on the anode side during Li-ion insertion, as depicted in Scheme 1e. This expansion led to significant increases in both pore volume (+2.5 × 10^5 $μm^3$), from 1.9 × 10^5 to 4.4 × 10^5 $μm^3$, and surface area (+0.7 × 10^6 $μm^2$), from 0.4 × 10^6 to 1.1 × 10^6 $μm^2$, within the analyzed statistical region (Figure 3d, e). These adverse structural transformations of Si/C electrodes compromise their mechanical stability and exacerbate parasitic reactions during cycling, thereby shortening battery lifespan and raising safety risks.

Following prelithiation, the mechanical behavior of Si/C anodes shifted to a void-filling-dominated mode, as evidenced by limited swelling and a pronounced 14.4% reduction in porosity upon charging. This conversion can be attributed to the densified and homogenized alloying reactions of prelithiated Si/C particles. Mechanically, the pre-expansion induced by prelithiation augmented the anode's void space (e.g., from 1.9 × 10^5 $μm^3$ to 2.9 × 10^5 $μm^3$ in the selected region). Coupled with the reduced rigidity of the prelithiated Si-based material [33, 41], this structural transformation of the anode enhanced its capability to accommodate inner stress-induced volume changes. Kinetically, the Li^+ diffusion coefficient of the Si/C electrode during charge/discharge increased from 4.0/3.6 to 5.5/4.8 × 10^{-11} cm^2 s^{-1} post-prelithiation (Figure S6), highlighting the improved transport kinetics of the pre-Si/C electrode. These improvements enabled the pre-Si/C electrode to withstand volume fluctuations while ensuring uniform electrochemical reactions across the entire large-scale electrode during repeated alloying/dealloying processes. Accordingly, the pore volume of the pre-Si/C anode exhibited a considerable reduction (-1.6 × 10^5 μ m^3) after charging, accompanied by a decrease in surface area (-0.1 × 10^6

μ m^2). The synergy between pre-expansion and material softening ultimately enables the pore-filling mechanism observed during the charging process of the prelithiated Si/C anode. Consequently, the structural integrity of the Si-based batteries is maintained, leading to stable and safe battery operation.

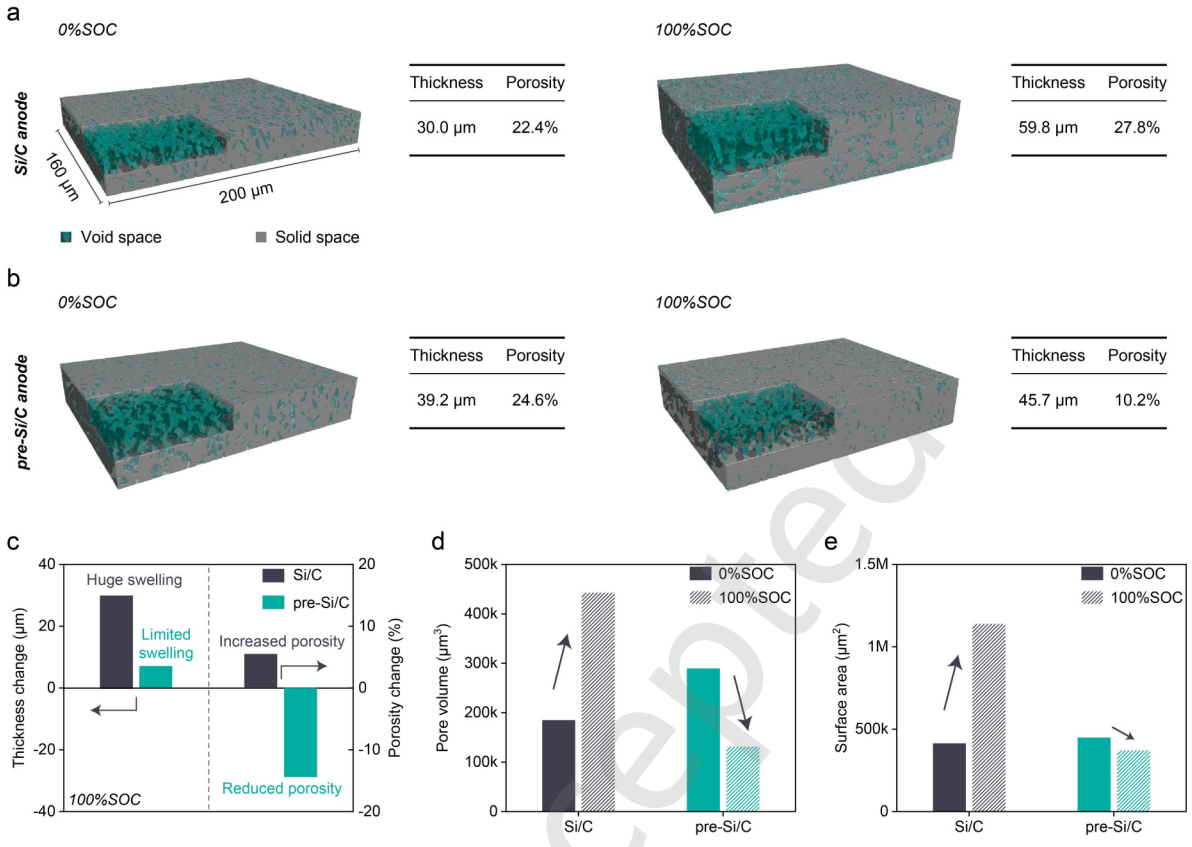

Figure 3. Structural evolution of Si-based anodes with and without prelithiation. (a, b) 3D renderings of a subvolume of the anode (~2.3 mAh cm^{-2}) for **(a)** LCO||Si/C and **(b)** LCO||pre-Si/C pouch cells at 0% and 100%SOC during the initial cycle at 0.1 *C*. The void space is shown in green, and the solid space in gray. The constituency area is identical, with dimensions of 160 × 200 μm. **(c)** Variations in thickness and porosity of the Si/C and pre-Si/C anodes after the initial lithiation. **(d)** Pore volume and **(e)** surface area within the Si/C and pre-Si/C anodes, at 0% and 100%SOC upon the first cycle.

2.5 *Electrochemical-mechanical behavior of LCO||Si/C pouch cells during operation*

The stress evolution of LCO||Si/C pouch cells during the initial 30 cycles at 0.5 *C* was monitored to investigate the role of prelithiation in modulating the volume effect during cycling. In cells utilizing a pristine Si/C anode, enormous and erratic pressure swings exceeding 85 kPa were observed during charging and discharging, despite a notably reduced cycling capacity (145.2 mAh in the initial cycle) relative to the rated value (Figure 4a and Figure S7). In contrast, the cell with the pre-Si/C electrode exhibited an elevated initial discharge capacity (213.7 mAh) and remarkably stable stress evolution, with stress fluctuations constrained to below 20 kPa throughout cycling (Figure 4b). The simultaneously increased capacity and decreased pressure variation highlight the efficacy of anode prelithiation in boosting energy density and structural durability of Si-based lithium-ion batteries. In the LCO||Si/C pouch cell, the average ΔP at the fully charged state reached 74.9 and 113.0 kPa in the 1st and 30th cycles at 0.5 *C*, respectively, corresponding to a high dP/dQ of 0.48 and 0.60 kPa mAh^{-1} (Figure 4c and Figure S8). Additionally, the distribution of ΔP across the entire Si/C anode was highly disordered (Figure 4d and Figure S9), with SD values of 358.9 and 380.3, reflecting heterogeneous electrochemical reactions during cycling. These indicate that the Si/C anode experienced substantial and disordered thickness expansion, which leads to interfacial degradation and side reactions. However, in the LCO||pre-Si/C pouch cell, both the average dP/dQ and SD values of ΔP significantly decreased and remained stable throughout the cycling, approaching 0.08 kPa mAh^{-1} and 18.3, respectively. These results validate the sustained efficacy of prelithiation in mitigating volume expansion and improving reaction homogeneity across large-scale Si-based electrodes.

Impedance analysis and morphological characterization were conducted to further assess the effect of prelithiation on the structural stability of Si-based anodes. As depicted in Figure 4e, the LCO||Si/C pouch cell exhibited increased resistance regarding the solution, interface, and charge transfer after 30 cycles at 0.5 *C*, compared to the first cycle (Table S2). This degradation is attributed to the development of a cracked and loose electrode structure (Figure 4f and Figure S10), stemming from the uncontrolled expansion/contraction of the Si/C anode. In contrast, cells incorporating the pre-Si/C anode exhibited consistently lower resistance, with only negligible growth after 30 cycles. Meanwhile, the pre-Si/C electrode retained an intact, smooth surface morphology and a dense electrode structure with no notable expansion (Figure 4g and Figure S11). Furthermore, this favorable structural integrity persisted over a long cycling (Figure S12), ensuring the mechanical robustness and safe operation of the Si-based battery. These findings underscore the role of prelithiation in enhancing the electrochemical-

mechanical stability of Si-based anodes.

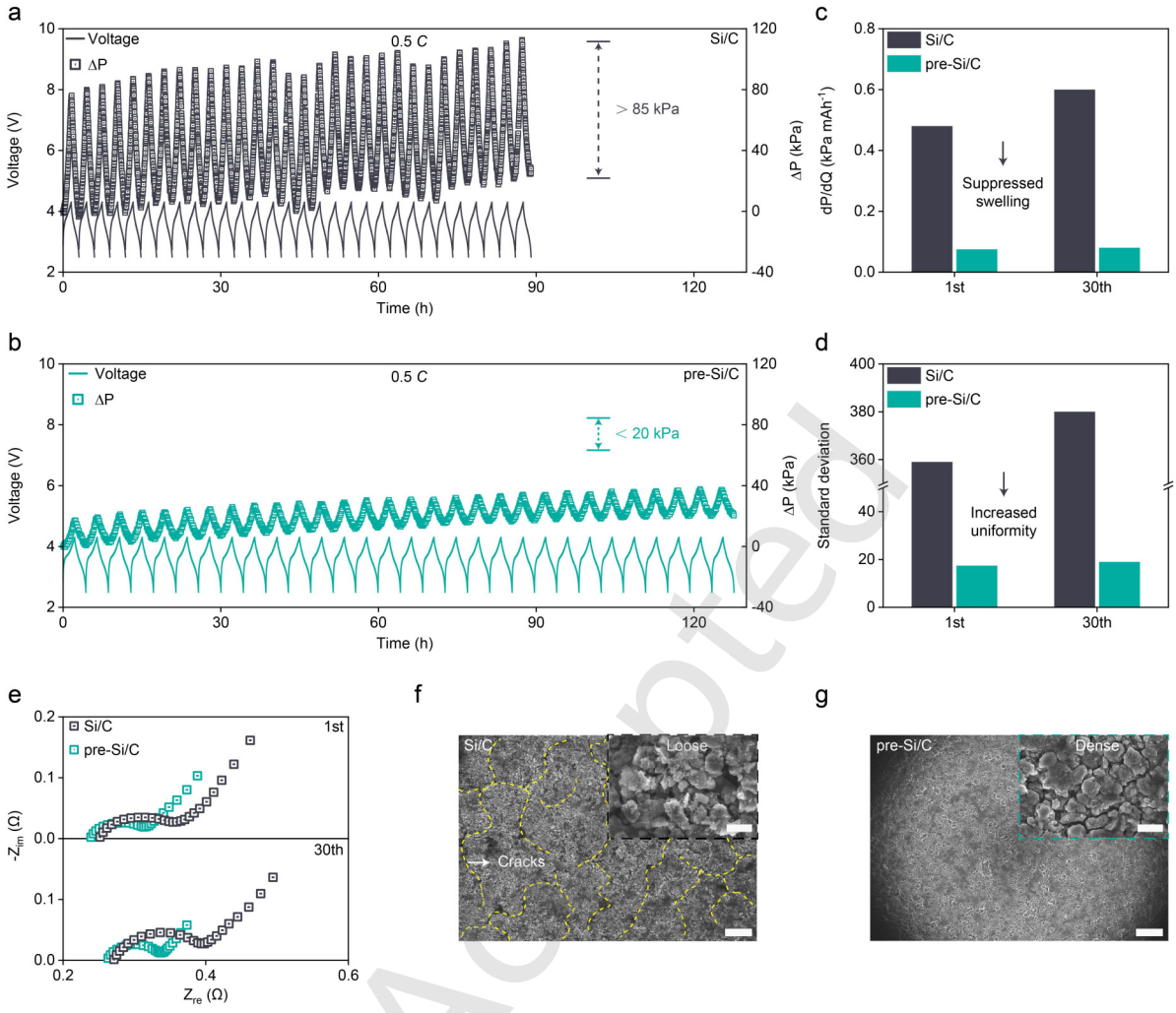

Figure 4. Electrochemical-mechanical behavior of LCO||Si/C laminated pouch cells during cycling. (a, b) Operando pressure measurement of the LCO||Si/C laminated pouch cell during the initial 30 cycles at 0.5 *C*, **(a)** without and **(b)** with anode prelithiation. **(c)** Average dP/dQ and **(d)** Standard deviation of ΔP at 100%SOC versus cycle number for the cell cycled at 0.5 *C*, with and without anode prelithiation. **(e)** Nyquist plots of the cell, pre- and post-anode prelithiation, after various cycles at 0.5 *C*. **(f, g)** Top-view SEM images of the anodes following the 30th charge, **(f)** without and **(g)** with prelithiation. Insets show the corresponding high-resolution SEM images. Scale bars, 100 μm (low-resolution) and 10 μm (high-resolution).

2.6 Stress and strain analysis model of Si-based full pouch cells *Composition and structure analysis of the SEI*

X-ray photoelectron spectroscopy (XPS) was employed to analyze the composition of SEI on the Si/C and pre-Si/C anodes after 30 cycles at 0.5 *C*. In the high-resolution F 1*s* spectra, peaks corresponding to LiP_xF_y and LiF components were observed at 687.0 and 685 eV [42], respectively, on the surface of the cycled Si/C anode (Figure 5a). Notably, the cycled pre-Si/C anode exhibited a higher LiF peak and a lower LiP_xF_y peak compared to its unprelithiated counterpart (Figure 5b), indicating the formation of a LiF-rich SEI and suppressed electrolyte decomposition. Furthermore, the high-resolution P 2*p* XPS spectra of the cycled Si/C anode revealed the extensive presence of $LiPF_6$ decomposition products, including $Li_xPF_yO_2$ and Li_xPF_y, at 134.5 and 137.0 eV [43], respectively (Figure 5c). In comparison, the intensities of these two peaks significantly reduced on the cycled pre-Si/C anode, indicating the effective mitigation of $LiPF_6$ reduction during cycling (Figure 5d). The suppressed parasitic reactions can be attributed to the decreased porosity and surface area of the pre-Si/C anode during cycling (Figure 3c-e), a consequence of the prelithiation-tuned electrochemical-mechanical behavior.

Time-of-flight secondary ion mass spectrometry (ToF-SIMS) depth etching was further conducted to resolve the 3D nanostructure of SEI. LiF_2^- and C_2HO^- were identified as characteristic ionic fragments derived from LiF and organic components, respectively [44, 45]. After 30 cycles, a broad and disordered distribution of these two species was revealed, indicating the formation of a thick and irregular SEI on the cycled Si/C anode (Figure 5e, f). This result suggests heterogeneous electrochemical reactions, which deplete active Li and electrolyte, thereby accelerating SEI growth. Conversely, the pre-Si/C anode presented a thin and uniform SEI layer after 30 cycles under identical conditions, characterized by a narrow and homogeneous distribution of both LiF_2^- and C_2HO^- components. This indicates the suppression of interfacial degradation and the homogenization of alloying/dealloying reactions. Thus, the pre-Si/C electrode sustained a stable electrode-electrolyte interface, effectively mitigating electrolyte decomposition and excessive SEI growth, both of which are critical for enhancing the electrochemical performance of Si-

based batteries.

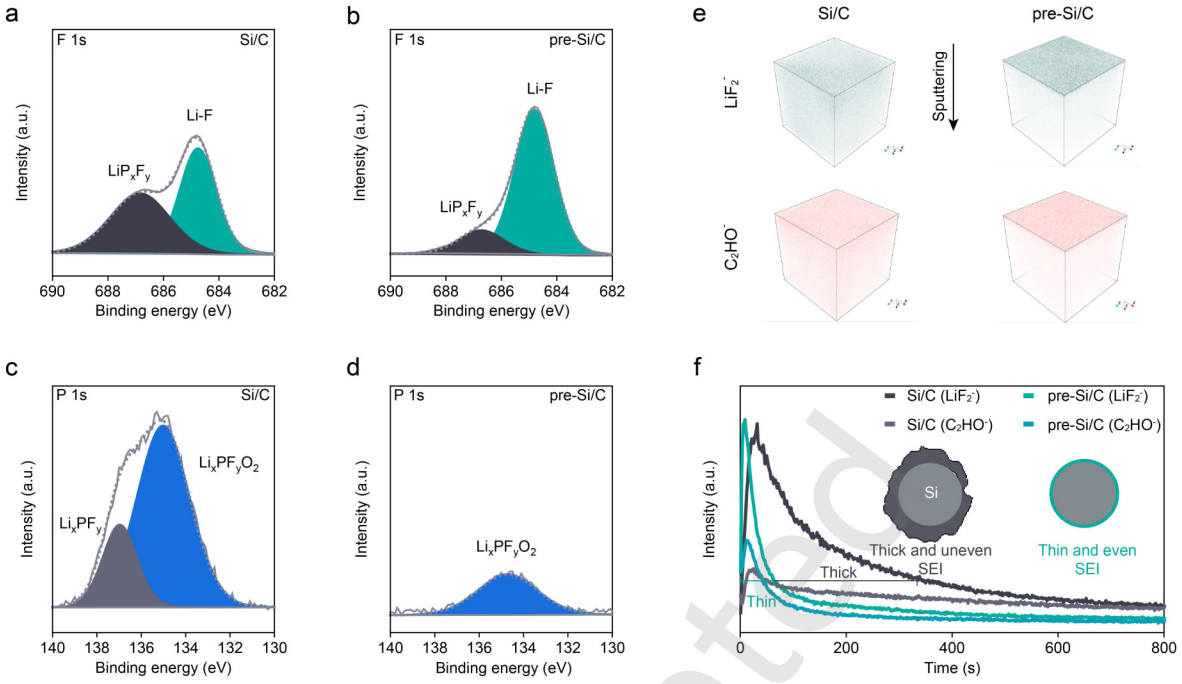

Figure 5. Composition and structure analysis of the SEI on cycled anodes. (a, b) High-resolution F 1*s* XPS spectra of **(a)** Si/C and **(b)** pre-Si/C anodes after 30 cycles at 0.5 *C*. **(c, d)** High-resolution P 2*p* XPS spectra of **(c)** Si/C and **(d)** pre-Si/C anodes after 30 cycles at 0.5 *C*. **(e)** 3D views of LiF_2^- (for LiF) and C_2HO^- (for organic components) in the ToF-SIMS sputtered volumes of the SEI on Si/C and pre-Si/C anodes after 30 cycles, and the corresponding **(f)** ToF-SIMS depth profiles.

2.7 *Influence of electrochemical-mechanical behavior on electrochemical performance*

To explore the influence of electrochemical–mechanical stability on electrochemical performance, we evaluated the cycling performance of 250 mAh-level LCO||Si/C pouch cells under practical conditions of a negative/positive capacity ratio of 1.1 and an electrolyte dosage of 3.0 g Ah^{-1}. As shown in Figure 6a, the LCO||pre-Si/C cell maintained 96.7% of its initial capacity after 100 cycles and 92.8% after 200 cycles at 0.5 *C*, corresponding to cumulative discharge capacities (representing the capability of energy export for a cell with rated capacity) of 21.2 and 41.5 Ah, respectively. Remarkably, even after 500 cycles, the LCO||pre-Si/C pouch cell retained 78.4% of its initial capacity, demonstrating exceptional long-term cycling performance. By contrast, the unprelithiated counterpart retained only 74.5% of its initial capacity after 100 cycles and 65.7% after 200 cycles, while exhibiting significant voltage hysteresis under identical conditions (Figure 6b, c). Despite having the same rated capacity, the cumulative discharge capacity of the unprelithiated LCO||Si/C cell sharply declined to 11.9 and 21.8 Ah after 100 and 200 cycles, respectively. Overall, anode prelithiation led to a 27.1% improvement in capacity retention and a 90.4% increase in cumulative discharge capacity for LCO||Si/C pouch cells after 200 cycles. These findings highlight the pivotal role of prelithiation in modulating the electrochemical-mechanical behavior of Si-based electrodes, thereby concurrently enhancing cycling stability and energy density.

To comprehensively assess the influence of electrochemical-mechanical behavior on cell performance, we present a stress/strain evolution diagram for practical LCO||Si/C pouch cells in Figure 6d. During cycling at 0.5 *C*, the thickness of the Si/C anode expanded from ~30 μm to ~78, 106, and 127 μm after the 1st, 30th, and 100th charge cycles, respectively. Correspondingly, the ΔP within the LCO||Si/C pouch cell accumulated to 74.3, 111.4, and 135.9 kPa, respectively. Besides, the average thickness change per cycle (ΔT) decreased from 0.97 μm (from the 1st to the 30th cycle) to 0.30 μm (from the 30th to the 100th cycle), exhibiting a slowdown in expansion. This phenomenon is attributed to increased electrode porosity and reduced Li capacity during cycling, which collectively suppress lithiation-induced thickness growth. In contrast, the LCO||pre-Si/C pouch cell demonstrated well-controlled growth in both stress and strain. From the 1st to 100th cycle, the thickness of the pre-Si/C anode increased by only ~9 μm, which is less than one-fifth of the ~49 μm expansion observed in the Si/C anode. A similar decelerated growth in anode thickness was also observed, with a small average ΔT per cycle, decreasing from 0.17 μm (from the 1st to the 30th cycle) to 0.06 μm (from the 30th to the 100th cycle). Simultaneously, the LCO||pre-Si/C pouch cell displayed significantly reduced ΔP throughout cycling, with values of 19.5, 37.5, and 46.7 kPa at the 1st, 30th, and 100th fully charged states, respectively. These results underscore the critical role of prelithiation in mitigating the volume expansion and enhancing electrochemical-mechanical stability for Si-based electrodes.

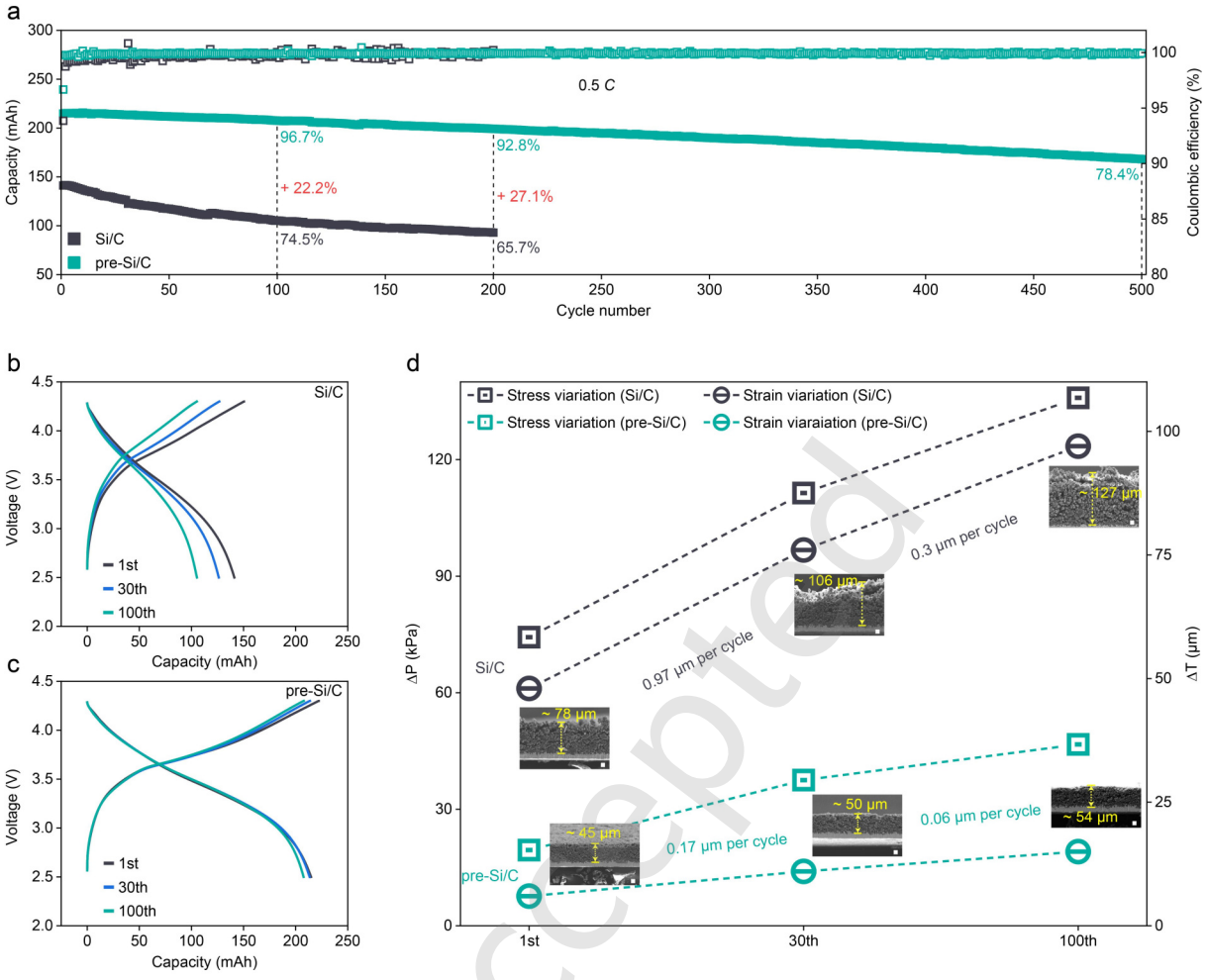

Figure 6. Electrochemical performance of LCO||Si/C laminated pouch cells. (a) Cell capacity and coulombic efficiency (CE) versus cycle number for LCO||Si/C and LCO||pre-Si/C laminated pouch cells, charged/discharged at 0.5 *C*. **(b, c)** Voltage profiles of the cell **(b)** without and **(c)** with anode prelithiation at the 1st, 30th, and 100th cycles. **(d)** A stress-strain evolution diagram for LCO||Si/C laminated pouch cells with and without anode prelithiation during cycling. Scale bars, 10 μm.

3 Conclusions

In this contribution, we elucidated the electrochemical-mechanical behavior and inner stress-driven structural evolution mechanism of Si-based anodes using an LCO||Si/C pouch cell configuration. Significant and disordered volume expansion, experienced by the high-capacity Si-based anode during charging, resulted in a mechanically unstable electrode structure with increased porosity, thereby compromising electrochemical performance. Critically, we unveiled the essential yet overlooked role of prelithiation in regulating the electrochemical-mechanical behavior of Si-based anodes. Prelithiation shifts the stress-induced structural swelling of the anode toward a void-filling-dominated pattern, which exploits inner stress to densify electrode structure during lithiation, contributing to a restricted volume expansion with high homogeneity. This is evidenced by a notable 14.4% reduction in anode porosity during the initial charge at 0.1 *C*, compared to a 5.4% increase observed in the unprelithiated counterpart. Simultaneously, electrode thickness expansion was significantly suppressed, decreasing from over 153% to below 18%. As a result, capacity retention improved by 27.1%, while cumulative discharge capacity increased by 90.4% after 200 cycles at 0.5 *C* in a full pouch cell configuration (8 × 8 cm). This study marks a significant step towards comprehending the stress-induced structural evolution of high-capacity electrodes during cycling, and sheds light on the effect of prelithiation in modulating the volume response of Si-based anodes in high-energy-density batteries.

Electronic Supplementary Material: Supplementary material (please provide the brief detail of the ESM) is available in the online version of this article at https://doi.org/10.26599/NR.2026.94908467.

Data availability

Data supporting the findings of this study are available from the corresponding author upon reasonable request.

Acknowledgements

This work is financially supported by the Natural Science Foundation of China (Grant No. 52272207). The authors would like to thank the Analytical and Testing Center of Huazhong University of Science and Technology (HUST) for providing the facilities to conduct the characterizations.

Declaration of competing interest

The authors declare no competing financial interest.

Author contribution statement

Y.S., X.D., and Y.O. conceived the idea and designed the experiments for this work. X.D. and Y.O. performed the material characterizations, mechanical and electrochemical measurements with assistance from S.T., W.W., H.S., G.L., Y.L., J.F., R.F., and R.Z. X.D. wrote the original paper. Y.S. reviewed and edited the paper.

Informed consent

None.

Ethics statement

None.

Use of AI statement

None.

References

[1] Choi, S.; Kwon, T.-w.; Coskun, A.; Choi, J. W. Highly elastic binders integrating polyrotaxanes for silicon microparticle anodes in lithium ion batteries. *Science* **2017**, 357, 279-283.

[2] Jin, Y.; Zhu, B.;Lu, Z.; Liu, N.; Zhu, J. Challenges and Recent Progress in the Development of Si Anodes for Lithium‐Ion Battery. *Adv. Energy Mater.* **2017**, 7, 1700715.

[3] Cui, Y. Silicon anodes. Silicon anodes. *Nat. Energy* **2021**, *6, 995-996.*

[4] Yu, P.; Li, Z.; Zhang, D.; Xiong, Q.; Yu, J.; Zhi, C. Hierarchical Yolk‐Shell Silicon/Carbon Anode Materials Enhanced by Vertical Graphene Sheets for Commercial Lithium‐Ion Battery Applications. *Adv. Funct. Mater.* **2025**, 35, 2413081.

[5] Wang, C.; Wu, H.; Chen, Z.;McDowell, M. T.;Cui, Y.; Bao, Z. Self-healing chemistry enables the stable operation of silicon microparticle anodes for high-energy lithium-ion batteries. *Nat. Chem.* **2013**, 5, 1042-1048.

[6] Pomerantseva, E.; Bonaccorso, F.; Feng, X.; Cui, Y.; Gogotsi, Y. Energy storage: The future enabled by nanomaterials. *Science* **2019**, 366, eaan8285.

[7] Ye, L.; Lu, Y.; Wang, Y.;Li, J.; Li, X. Fast cycling of lithium metal in solid-state batteries by constriction-susceptible anode materials. *Nat. Mater.* **2024**, 23, 244-251.

[8] Chen, Z.; Soltani, A.; Chen, Y.; Zhang, Q.; Davoodi, A.; Hosseinpour, S.; Peukert, W.; Liu, W. Emerging Organic Surface Chemistry for Si Anodes in Lithium‐Ion Batteries: Advances, Prospects, and Beyond. *Adv. Energy Mater.* **2022**, 12, 2200924.

[9] Kim, N.; Kim, Y.; Sung, J.; Cho, J. Issues impeding the commercialization of laboratory innovations for energy-dense Si-containing lithium-ion batteries. *Nat. Energy* **2023**, 8, 921-933.

[10] Liu, N.;Lu, Z.;Zhao, J.;McDowell, M. T.;Lee, H.-W.;Zhao, W.; Cui, Y. A pomegranate-inspired nanoscale design for large-volume-change lithium battery anodes. *Nat. Nanotechnol.* **2014**, 9, 187-192.

[11] Sung, J.; Kim, N.; Ma, J.;Lee, J. H.; Joo, S. H.; Lee, T.; Chae, S.; Yoon, M.; Lee, Y.; Hwang, J.; Kwak, S. K.; Cho, J. Subnano-sized silicon anode via crystal growth inhibition mechanism and its application in a prototype battery pack. *Nat. Energy* **2021**, 6, 1164-1175.

[12] Xu, D. X.; Zhao, Y. M.; Chen, H. X.; Lu, Z. Y.; Tian, Y. F.; Xin, S.; Li, G.; Guo, Y. G. Reduced Volume Expansion of Micron‐Sized SiOx via Closed‐Nanopore Structure Constructed by Mg‐Induced Elemental Segregation. *Angew. Chem. Int. Ed.* **2024**, 63, e202401973.

[13] Kwon, T.-w.; Choi, J. W.; Coskun, A. Prospect for Supramolecular Chemistry in High-Energy-Density Rechargeable Batteries. *Joule* **2019**, 3, 662-682.

[14] Lin, J.; Wang, L.; Xie, Q.; Luo, Q.; Peng, D. L.;Buddie Mullins, C.; Heller, A. Stainless Steel‐Like Passivation Inspires Persistent Silicon Anodes for Lithium‐Ion Batteries. *Angew. Chem. Int. Ed.* **2023**, 135, e202216557.

[15] He, Z.; Zhang, C.; Zhu, Y.; Wei, F. The acupuncture effect of carbon nanotubes induced by the volume expansion of silicon-based anodes. *Energy Environ. Sci.* **2024**, 17, 3358-3364.

[16] Li, C.; Wang, J.; Wang, X.; Chen, Z.;Zhan, R.; Duan, X.; Liu, X.;Cheng, K.;Cai, Z.; Wang, L.; Sun, Y. Regulating the mechano-electrochemistry of graphite-silicon hybrid anode through layered electrode structure design. *J. Energy Chem.* **2025**, 104, 176-184.

[17] Li, A.-M.; Wang, Z.; Lee, T.; Zhang, N.; Li, T.;Zhang, W.; Jayawardana, C.; Yeddala, M.; Lucht, B. L.; Wang, C. Asymmetric electrolyte design for high-energy lithium-ion batteries with micro-sized alloying anodes. *Nat. Energy* **2024**, 9, 1551-1560.

[18] Liu, T.; Dong, T.; Wang, M.; Du, X.; Sun, Y.; Xu, G.; Zhang, H.; Dong, S.; Cui, G. Recycled micro-sized silicon anode for high-voltage lithium-ion batteries. *Nat. Sustainability* **2024**, 7, 1057-1066.

[19] Je, M.; Han, D.-Y.; Ryu, J.; Park, S. Constructing Pure Si Anodes for Advanced Lithium Batteries. *Acc. Chem. Res.* **2023**, 56, 2213-2224.

[20] Zhao, H.; Li, J.;Zhao, Q.; Huang, X.; Jia, S.; Ma, J.; Ren, Y. Si-Based Anodes: Advances and Challenges in Li-Ion Batteries for Enhanced Stability. *Electrochem. Energy Rev.* **2024**, 7, 11.

[21] Xiao, Z.; Wu, H.; Quan, L.; Zeng, F.; Guo, R.; Ma, Z.; Chen, X.; Zhan, J.;Xu, K.; Xing, L.; Li, W. Micro-sized CVD-derived Si–C anodes: challenges, strategies, and prospects for next-generation high-energy lithium-ion batteries. *Energy Environ. Sci.* **2025**, 18, 4037-4052.

[22] Eshetu, G. G.; Zhang, H.; Judez, X.; Adenusi, H.; Armand, M.;Passerini, S.; Figgemeier, E. Production of high-energy Li-ion batteries comprising silicon-containing anodes and insertion-type cathodes. *Nat. Commun.* **2021**, 12, 5459.

[23] Ge, C.; Xu, D.; Feng, X.; Yang, X.; Song, Z.; Song, Y.; Chen, J.; Liu, Y.; Gao, C.; Du, Y.; Sun, Z.; Xu, W.; Fang, J. Recent Advances in Fibrous Materials for Hydroelectricity Generation. *Nano-micro Lett.* **2024**, 17, 29.

[24] Jia, P.; Guo, J.; Li, Q.; Liu, Y.; Zheng, Y.; Guo, Y.;Huang, Y.; Shen, Y.;Long, L.; Zhang, H.; Chen, R.; Zhang, C.; Zhang, Z.; Shen, J.; Dong, S.; Jiang, J.; Chang, M.; Liu, X.; Wang, X.; Tang, Y.; Shao, H. Revisiting the kinetics enhancement strategies of Si anodes through deconstructing particle–interface–electrode integration. *Energy Environ. Sci.* **2025**, 18, 2720-2746.

[25] Wang, X.; Chen, Z.; Liu, S.; Tu, S.;Zhan, R.; Wang, L.; Sun, Y. Anode interphase design for fast-charging lithium-based rechargeable batteries. *Energy Environ. Sci.* **2025**, 18, 2648-2667.

[26] Zhang, Y.; Xiao, X.; Chen, W.; Zhang, Z.; Li, W.; Ge, X.;Li, Y.; Xiang, J.;Sun, Q.;Yan, Z.; Yu, Y.; Yang, H.; Li, Z.; Huang, Y. In Operando Monitoring the Stress Evolution of Silicon Anode Electrodes during Battery Operation via Optical Fiber Sensors. *Small* **2024**, 20, 2311299.

[27] Cao, Z.; Sun, H.; Zhang, Y.;Yuan, L.; Liao, Y.; Ji, H.; Hao, S.; Li, Z.; Qie, L.; Huang, Y. Metallized polymer current collector as “stress acceptor” for stable micron-sized silicon anodes. *J. Energy Chem.* **2025**, 101, 786-794.

[28] Louli, A. J.; Ellis, L. D.; Dahn, J. R. Operando Pressure Measurements Reveal Solid Electrolyte Interphase Growth to Rank Li-Ion Cell Performance. *Joule* **2019**, 3, 745-761.

[29] Dressler, R. A.; Dahn, J. R. Investigation of The Failure Mechanisms of Li-Ion Pouch Cells with Si/Graphite Composite Negative Electrodes and Single Wall Carbon Nanotube Conducting Additive. *J. Electrochem. Soc.* **2024**, 171, 030532.

[30] Koyama, Y.; Chin, T. E.; Rhyner, U.;Holman, R. K.; Hall, S. R.; Chiang, Y. M. Harnessing the Actuation Potential of Solid‐State Intercalation Compounds. *Adv. Funct. Mater.* **2006**, 16, 492-498.

[31] Huang, W.; Ye, Y.;Chen, H.; Vilá, R. A.; Xiang, A.; Wang, H.; Liu, F.; Yu, Z.; Xu, J.; Zhang, Z.; Xu, R.; Wu, Y.;Chou, L.-Y.; Wang, H.; Xu, J.;Boyle, D. T.; Li, Y.; Cui, Y. Onboard early detection and mitigation of lithium plating in fast-charging batteries. *Nat. Commun.* **2022**, 13, 7091.

[32] Berla, L. A.; Lee, S. W.; Cui, Y.; Nix, W. D. Mechanical behavior of electrochemically lithiated silicon. *J. Power Sources* **2015**, 273, 41-51.

[33] Tan, D. H. S.; Chen, Y.-T.; Yang, H.;Bao, W.; Sreenarayanan, B.; Doux, J.-M.; Li, W.;Lu, B.; Ham, S.-Y.;Sayahpour, B.; Scharf, J.; Wu, E. A.;Deysher, G.; Han, H. E.; Hah, H. J.; Jeong, H.; Lee, J. B.; Chen, Z.; Meng, Y. S. Carbon-free high-loading silicon anodes enabled by sulfide solid electrolytes. *Science* **2021**, 373, 1494-1499.

[34] Hertzberg, B.;Benson, J.; Yushin, G. Ex-situ depth-sensing indentation measurements of electrochemically produced Si–Li alloy films. *Electrochem. Commun.* **2011**, 13, 818-821.

[35] Zhan, R.; Wang, X.; Chen, Z.; Seh, Z. W.; Wang, L.; Sun, Y. Promises and Challenges of the Practical Implementation of Prelithiation in Lithium‐Ion Batteries. *Adv. Energy Mater.* **2021**, 11, 2101565.

[36] Ou, Y.; Zhang, B.; Zhan, R.; Liu, S.; Wang, W.; Tu, S.; Hu, Y.; Chen, Z.; Duan, X.; Wang, X.; Wang, L.; Sun, Y. A salt-free medium facilitating electrode prelithiation towards fast-charging and high-energy lithium-ion batteries. *Nat Commun* **2025**, 16, 7956.

[37] Ou, Y.; Zhan, R.; Liu, S.; Shen, H.; Wang, W.; Tu, S.; Duan, X.; Chen, Z.; Wang, X.; Feng, R.; Fu, J.; Chen, X.; Li, C.; Tan, Y.; Cheng, K.; Liu, S.; Sun, Y. Solvent–Mediated Cathode Prelithiation for Durable, High‐Energy Lithium‐Ion Batteries. *Adv. Funct. Mater.* **2025**, e21473, 10.1002/adfm.202521473.

[38] Ye, Y.; Xu, R.; Huang, W.; Ai, H.; Zhang, W.; Affeld, J. O.; Cui, A.; Liu, F.; Gao, X.; Chen, Z.; Li, T.;Xiao, X.;Zhang, Z.;Peng, Y.;Vila, R. A.;Wu, Y.;Oyakhire, S. T.;Kuwajima, H.;Suzuki, Y.;Matsumoto, R.;Masuda, Y.;Yuuki, T.;Nakayama, Y.; Cui, Y. Quadruple the rate capability of high-energy batteries through a porous current collector design. *Nat. Energy* **2024**, 9, 643-653.

[39] Vanpeene, V.; King, A.; Maire, E.; Roué, L. In situ characterization of Si-based anodes by coupling synchrotron X-ray tomography and diffraction. *Nano Energy* **2019**, 56, 799-812.

[40] Sandoval, S. E.; Lewis, J. A.; Vishnugopi, B. S.; Nelson, D. L.;Schneider, M. M.; Cortes, F. J. Q.;Matthews, C. M.;Watt, J.;Tian, M.;Shevchenko, P.;Mukherjee, P. P.; McDowell, M. T. Structural and electrochemical evolution of alloy interfacial layers in anode-free solid-state batteries. *Joule* **2023**, 7, 2054-2073.

[41] Zhang, Z.; Sun, Z.; Han, X.; Liu, Y.; Pei, S.;Li, Y.; Luo, L.; Su, P.; Lan, C.; Zhang, Z.; Xu, S.; Guo, S.; Huang, W.; Chen, S.; Wang, M.-S. An all-electrochem-active silicon anode enabled by spontaneous Li–Si alloying for ultra-high performance solid-state batteries. *Energy Environ. Sci.* **2024**, 17, 1061-1072.

[42] Chen, J.; Fan, X.; Li, Q.; Yang, H.; Khoshi, M. R.; Xu, Y.; Hwang, S.; Chen, L.; Ji, X.; Yang, C.; He, H.; Wang, C.; Garfunkel, E.; Su, D.;Borodin, O.; Wang, C. Electrolyte design for LiF-rich solid–electrolyte interfaces to enable high-performance microsized alloy anodes for batteries. *Nat. Energy* **2020**, 5, 386-397.

[43] Cheng, K.; Tu, S.; Zhang, B.; Wang, W.; Wang, X.; Tan, Y.; Chen, X.; Li, C.; Li, C.; Wang, L.; Sun, Y. Material–electrolyte interfacial interaction enabling the formation of an inorganic-rich solid electrolyte interphase for fast-charging Si-based lithium-ion batteries. *Energy Environ. Sci.* **2024**, 17, 2631-2641.

[44] Bai, M.; Tang, X.; Zhang, M.; Wang, H.; Wang, Z.; Shao, A.; Ma, Y. An in-situ polymerization strategy for gel polymer electrolyte Si||Ni-rich lithium-ion batteries. *Nat. Commun.* **2024**, 15, 5375.

[45] Bai, S.; Bao, W.; Qian, K.; Han, B.; Li, W.; Sayahpour, B.; Sreenarayanan, B.; Tan, D. H. S.; Ham, S. y.; Meng, Y. S. Elucidating the Role of Prelithiation in Si‐based Anodes for Interface Stabilization. *Adv. Energy Mater.* **2023**, 13, 2301041.

Electronic Supplementary Material

Understanding and regulation of stress-induced structural evolution in silicon anodes for high-energy-density batteries

Xiangrui Duan[§], Yangtao Ou[§], Shuibin Tu, Wenyu Wang, Hengtao Shen, Guocheng Li, Yuanjian Li, Junjie Fu, Ruikang Feng, Renming Zhan, and Yongming Sun ✉

Wuhan National Laboratory for Optoelectronics, Huazhong University of Science and Technology, Wuhan, 430074, China
[§] Xiangrui Duan and Yangtao Ou contributed equally to this work.

✉ Address correspondence to yongmingsun@hust.edu.cn

Supporting information to https://doi.org/10.26599/NR.2026.94908467

METHODS

Electrodes preparation:

Full pouch cells were assembled using a silicon/carbon (Si/C) anode and a $LiCoO_2$ (LCO) cathode throughout this work. The Si/C anode was prepared by mixing Si/C, carbon black, and lithium polyacrylate in water at a weight ratio of 8:1:1, followed by coating the slurry onto copper foil using a doctor blade process. Next, the electrodes were dried under vacuum at 80 °C for 12 hours. The LCO cathode was fabricated by dispersing LCO powder, carbon black, and polyvinylidene fluoride in N-methylpyrrolidone at a weight ratio of 90:5:5. The resulting slurry was then coated onto aluminum foil with a doctor blade method and subsequently dried under vacuum at 80 °C for 12 hours. The mass loadings of the Si/C anode and LCO cathode were approximately 1.8 mg cm^{-2} and 11.5 mg cm^{-2}, respectively. The LCO cathode exhibited an areal capacity of ~2.1 mAh cm^{-2} within a voltage window of 3.0–4.5 V *vs.* Li^+ /Li. The Si/C anode delivered an areal capacity of ~2.3 mAh cm^{-2} and a specific capacity of ~1300 mAh g^{-1} within the voltage range of 0.01–1.0 V *vs.* Li^+ /Li. The prelithiated Si/C (pre-Si/C) anode, prepared via a contact prelithiation method, demonstrated an initial coulombic efficiency approaching 100%, outperforming the unprelithiated counterpart (~77%) (Figure S13). The selection of a ~25% prelithiation degree was primarily intended to fully compensate for the initial irreversible lithium loss in the Si/C anode. The prelithiation process was conducted in an Ar-filled glove box, with oxygen and moisture levels maintained below 0.5 ppm and 0.1 ppm, respectively, at an ambient temperature of 25 °C. The pristine Si/C electrode was brought into direct contact with a metallic Li foil. A controlled amount of fluoroethylene carbonate (0.1 mL cm^{-2} of electrode area) was carefully dripped onto the interface to serve as the prelithiation medium. The assembly was then tightly sandwiched between two glass plates and held for 6 hours to complete the prelithiation.

Pouch cell assembly:

One piece of double-side LCO cathode (dimensions of 7.8 × 7.8 cm) and two pieces of single-side Si/C anode (dimensions of 8 × 8 cm) were utilized to assemble the 250 mAh-level LCO||Si/C laminated pouch cells. The cathode–anode pairing yielded an N/P ratio of approximately 1.1. A polypropylene membrane with a thickness of 30 μm was employed as the separator in all pouch cells. The electrolyte consisted of 1 M $LiPF_6$ dissolved in a 1:1 volume ratio mixture of ethylene carbonate (EC) and diethyl carbonate (DEC), supplemented with 5 vol% fluoroethylene carbonate (FEC) and 1 vol% vinylene carbonate (VC) as additives. The electrolyte amount was controlled at 3.0 g Ah^{-1}. All cell fabrication operations were performed in an argon-filled glove box, where the concentrations of H_2O and O_2 were strictly maintained below 1 ppm.

Operando spatial pressure test:

Operando spatial pressure was monitored using a force-sensor array film (G-PMS, SMiTSense) comprising a precisely arranged grid of force sensors. For real-time spatial pressure measurements, the fabricated pouch cell was placed between the plates of a clamping apparatus pre-set to a target initial external pressure, as illustrated in Figure S1a. The force-sensor film was positioned between the stainless-steel wall and the pouch cell to capture pressure variations during battery operation. The cell testing protocol was synchronized with the operando pressure measurements. The initial pressure was adjusted by tightening a screw mechanism, while a spring pad was employed to accommodate cell volume changes during charge and discharge. The initial measurement pressure was set at approximately 0.5 MPa to achieve a balance between electrochemical performance and practical applicability in real battery systems. A higher preload force may induce mechanical damage to the cell, whereas a lower preload force can result in an unstable electrode–electrolyte interface.

Material characterizations:

Scanning electron microscopy (SEM) was performed using a GeminiSEM 300 field-emission instrument (Carl Zeiss, Germany) to examine the sample morphology. Time-of-flight secondary ion mass spectrometry (ToF-SIMS) was carried out with a ToF.SIMS 5 system (IONTOF GmbH, Germany) to analyze the chemical composition of the samples. X-ray computed tomography (CT) was

conducted using an Xradia 610 Versa (Carl Zeiss, Germany) at an operating voltage of 60 kV to investigate the internal structure, including thickness and porosity. The resulting 3D volumes were processed using Dragonfly software. X-ray photoelectron spectroscopy (XPS) measurements were conducted with an AXIS-ULTRA DLD-600W system (Shimadzu, Japan) employing Al Kα radiation. Prior to analysis, the cycled electrodes were disassembled and rinsed with DMC solvent in an argon-filled glove box (H_2O and O_2 < 1 ppm).

Electrochemical tests:

Galvanostatic charge/discharge measurements were carried out using a LAND battery tester. The 250 mAh-class LCO||Si/C laminated pouch cells were tested at 0.5 *C* in the voltage range of 2.5–4.3 V (*vs.* Li^+/Li) following three activation cycles at 0.1 *C* (1 *C* = 180 mA g^{-1}). Electrochemical impedance spectroscopy (EIS) was conducted on a Biologic VMP3 multichannel workstation over a frequency range of 100 mHz to 100 kHz at open-circuit potential.

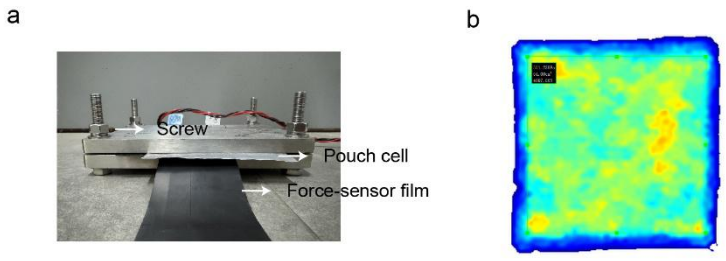

Figure S1. (a) Digital image of the operando spatial stress measurement setup. (b) Two-dimensional pressure distribution of the initially imposed pressure (~0.5 MPa) on the LCO||Si/C pouch cell.

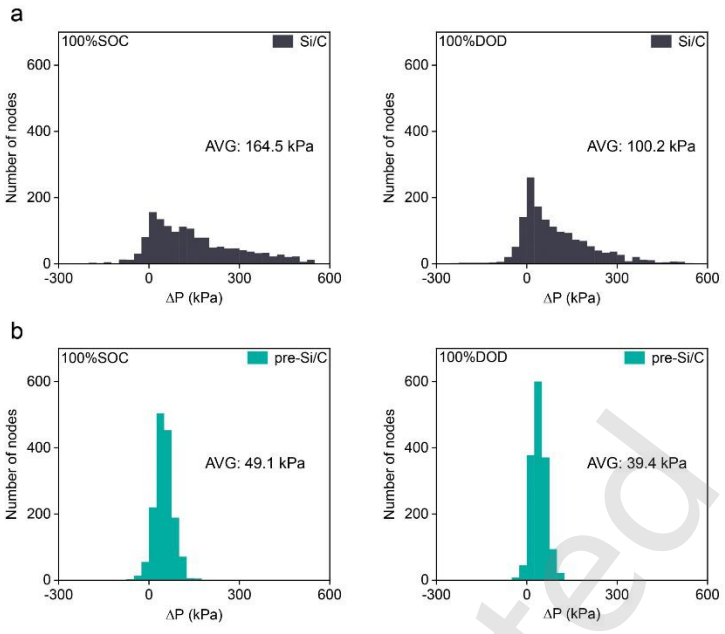

Figure S2. (a, b) Distribution histogram of ΔP for the (a) LCO||Si/C and (b) LCO||pre-Si/C pouch cells at 100% state of charge (SOC) and 100% depth of discharge (DOD) during the initial cycle at 0.1 *C*.

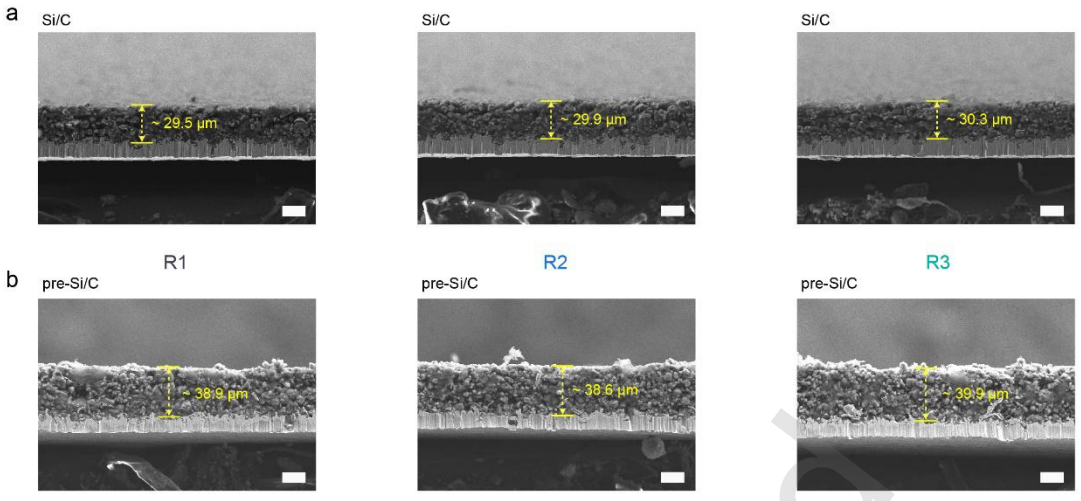

Figure S3. (a, b) Cross-sectional SEM images of the uncycled (a) Si/C and (b) pre-Si/C anodes, captured at three distinct regions: R1, R2, and R3. Scale bars, 20 μm.

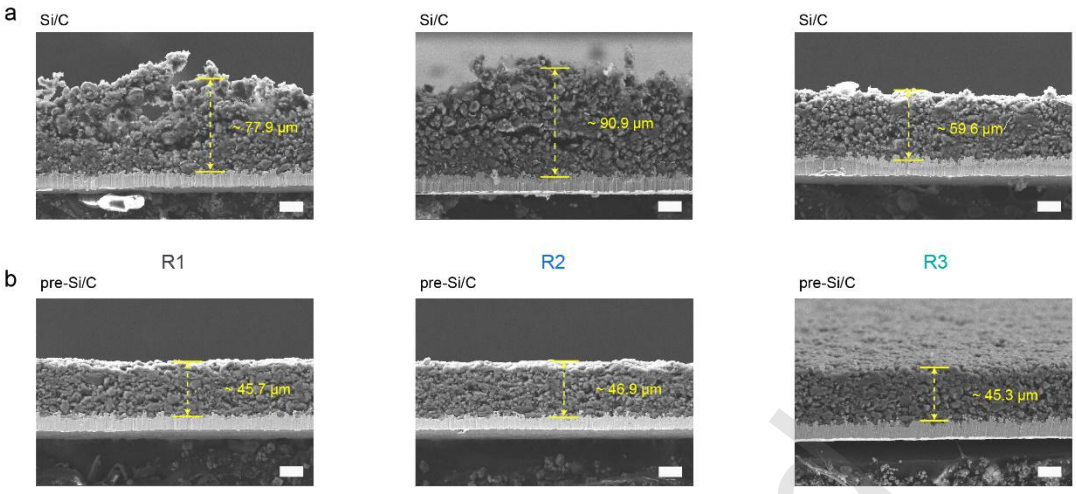

Figure S4. (a, b) Cross-sectional SEM images of the lithiated anodes from the (a) LCO||Si/C and (b) LCO||pre-Si/C pouch cells at 100%SOC, captured at three distinct regions: R1, R2, and R3. Scale bars, 20 μm.

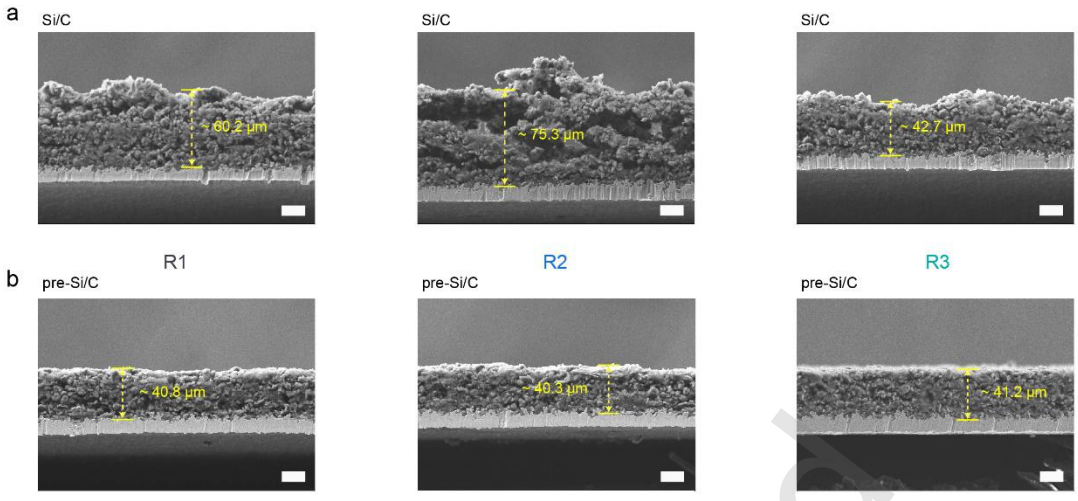

Figure S5. (a, b) Cross-sectional SEM images of the delithiated anodes from the (a) LCO||Si/C and (b) LCO||pre-Si/C pouch cells at 100%DOD, captured at three distinct regions: R1, R2, and R3. Scale bars, 20 μm.

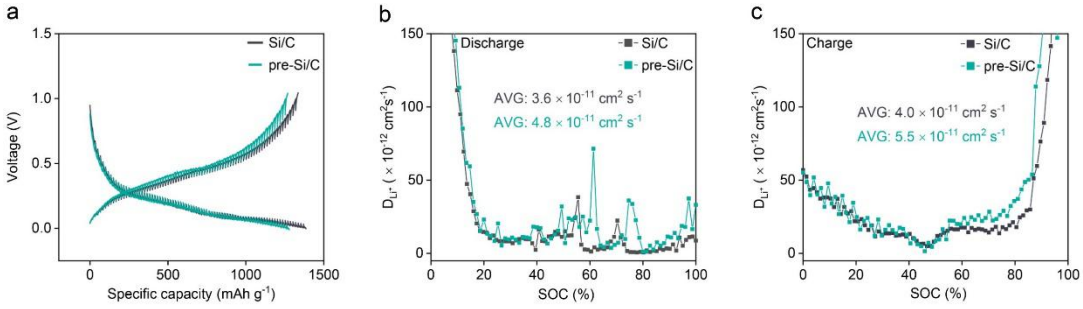

Figure S6. (a-c) Galvanostatic intermittent titration technique (GITT) tests for the Si/C and pre-Si/C electrodes: (a) capacity-potential curves, and D_{Li}^{+} calculated from the 3rd-cycle (b) discharge and (c) charge profiles.

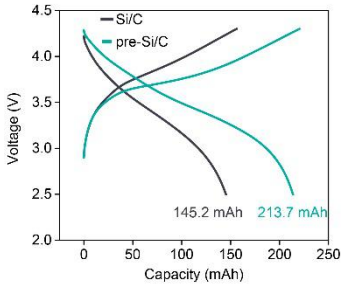

Figure S7. Voltage profiles of the LCO||Si/C and LCO||pre-Si/C cells during the initial cycle at 0.5 *C*.

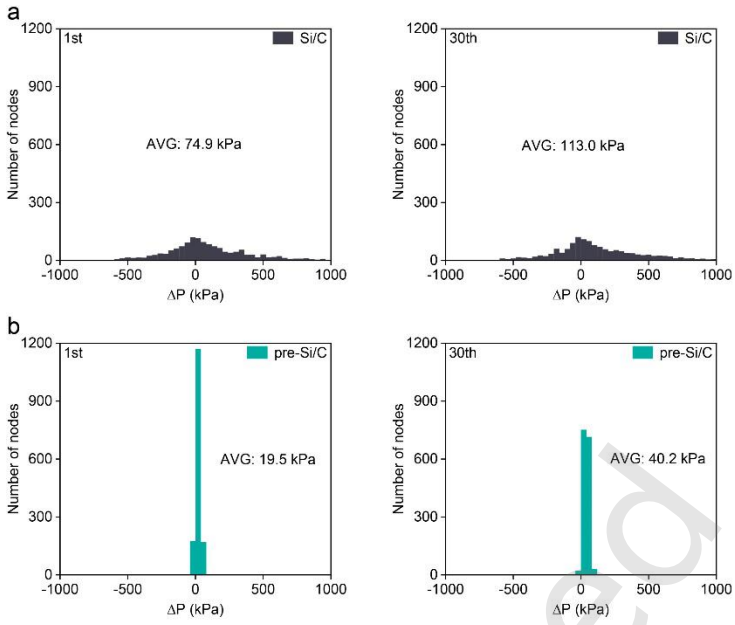

Figure S8. (a, b) Distribution histogram of ΔP for the (a) LCO||Si/C and (b) LCO||pre-Si/C pouch cells at 100%SOC during the 1st and 30th cycles at 0.5 *C*.

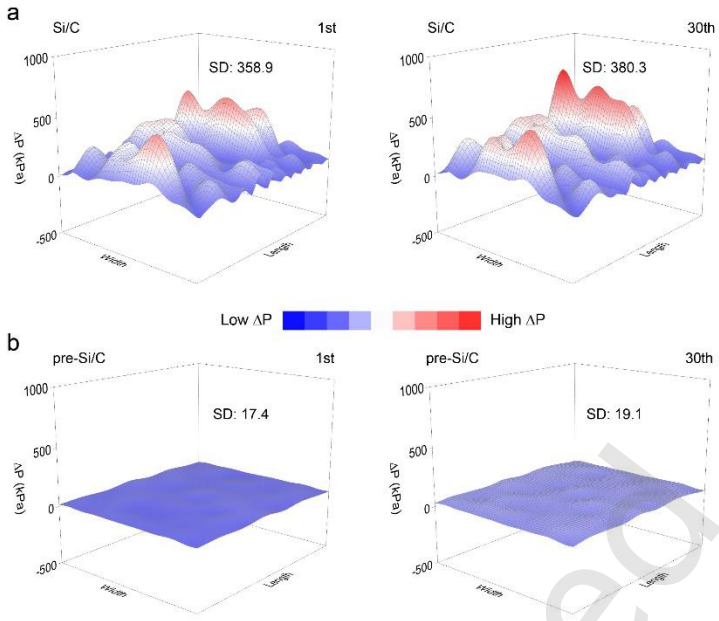

Figure S9. (a, b) Three-dimensional spatial distribution of ΔP for the (a) LCO||Si/C and (b) LCO||pre-Si/C pouch cells at 100%SOC during the 1st and 30th cycles at 0.5 *C*. Red represented higher ΔP than blue in the heat map.

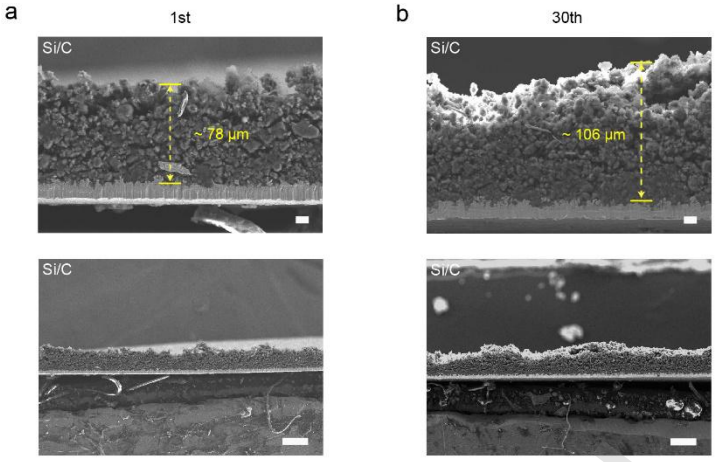

Figure S10. (a, b) High- and low-resolution cross-sectional SEM images of the lithiated anodes from the LCO||Si/C pouch cell at 100%SOC during the (a) 1st and (b) 30th cycles at 0.5 *C*. Scale bars, 10 µm (high-resolution) and 100 µm (low-resolution).

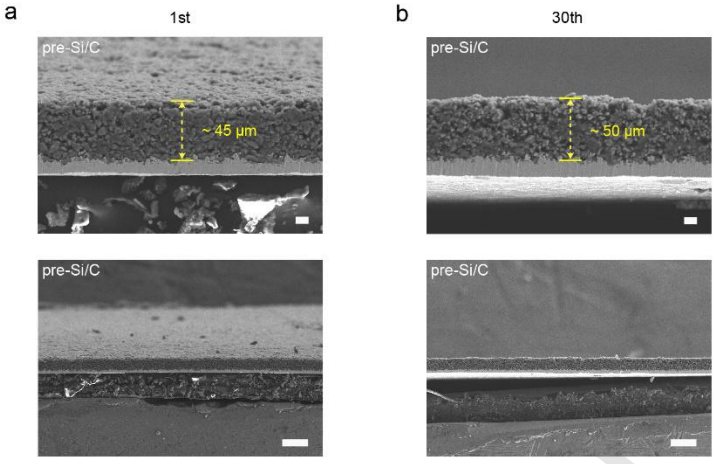

Figure S11. (a, b) High- and low-resolution cross-sectional SEM images of the lithiated anodes from the LCO||pre-Si/C pouch cell at 100%SOC during the (a) 1st and (b) 30th cycles at 0.5 *C*. Scale bars, 10 μm (high-resolution) and 100 μm (low-resolution).

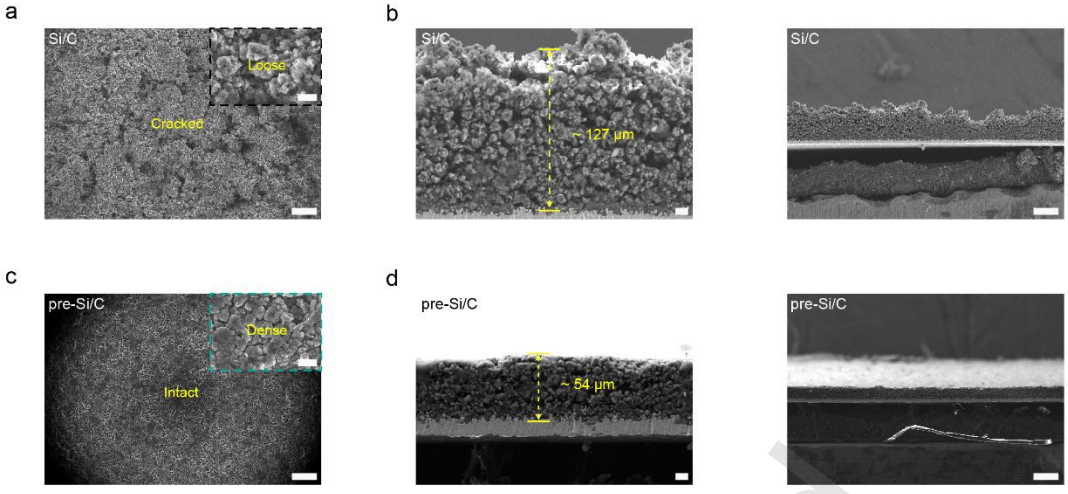

Figure S12. (a, b) High- and low-resolution (a) top-view and (b) cross-sectional SEM images of the lithiated anodes from the LCO||Si/C pouch cell at 100%SOC during the 100th cycle at 0.5 *C*. (c, d) High- and low-resolution (c) top-view and (d) cross-sectional SEM images of the lithiated anodes from the LCO||pre-Si/C pouch cell at 100%SOC during the 100th cycle at 0.5 *C*. Scale bars, 10 μm (high-resolution) and 100 μm (low-resolution).

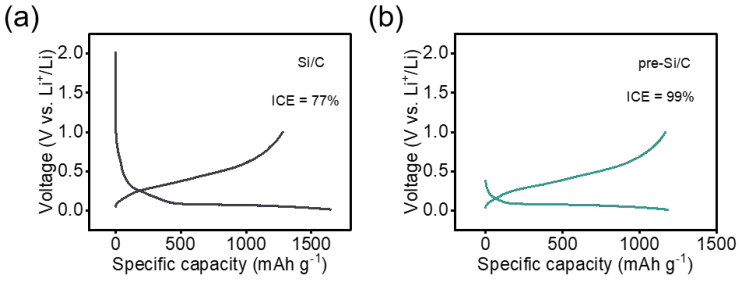

Figure S13. (a, b) The first-cycle voltage profile of (a) Si/C and (b) pre-Si/C anode at 0.1 C.

Table S1. Thickness change of the laminated Si-based full pouch cell before and after lithiation.

Cell component	Unit thickness (μm)	Number	Thickness (μm) (0%SOC)	Thickness (μm) (100%SOC)
NMC cathode	140	10	1400	1386 (reduce by ~1%)
Al current collector	13	10	130	130
Si-based anode	80	10	800	1600 (increase by ~100%)
Cu current collector	10	11	110	110
Separator	19	20	380	380
Al-plastic film	113	2	226	226
Cell	/	/	3046	3832 (increase by ~26%)

[a] The Si-based full pouch cell is configured with a Li capacity of ~4 mAh cm^{-2} (single side), an anode specific capacity exceeding 1000 mAh g^{-1}, and a lamination number of 10.

Table S2. Fitted values of the resistance, regarding the solution (R_s), the interface (R_i), and the charge transfer (R_{ct}), for LCO||Si/C and LCO||pre-Si/C pouch cells after 1 and 30 cycles at 0.5 *C*.

Cycle number (n)	Electrode	R_s (Ω)	R_i (Ω)	R_{ct} (Ω)
After 1 cycle	***Si/C***	0.25	0.06	0.08
	pre-Si/C	0.24	0.04	0.06
After 30 cycles	***Si/C***	0.27	0.13	0.12
	pre-Si/C	0.26	0.05	0.07